Performance analysis of two EM-based measurement bias estimation processes for tracking systems[*]

Zhi-hua LU[‡1], Meng-yao ZHU[2], Qing-wei YE[1], Yu ZHOU[1]

[1]College of Information Science and Engineering, Ningbo University, Ningbo 315211, China

[2]School of Communication and Information Engineering, Shanghai University, Shanghai 200072, China

E-mail: luzhihua@nbu.edu.cn; zhumengyao@shu.edu.cn; yeqingwei@nbu.edu.cn; zhouyu@nbu.edu.cn

Received Apr. 7, 2018; Revision accepted Sept. 24, 2018; Crosschecked Sept. 25, 2018

Abstract: In target tracking, the measurements collected by sensors can be biased in some real scenarios, e.g., due to systematic error. To accurately estimate the target trajectory, it is essential that the measurement bias be identified in the first place. We investigate the iterative bias estimation process based on the expectation-maximization (EM) algorithm, for cases where sufficiently large numbers of measurements are at hand. With the assistance of extended Kalman filtering and smoothing, we derive two EM estimation processes to estimate the measurement bias which is formulated as a random variable in one state-space model and a constant value in another. More importantly, we theoretically derive the global convergence result of the EM-based measurement bias estimation and reveal the link between the two proposed EM estimation processes in the respective state-space models. It is found that the bias estimate in the second state-space model is more accurate and of less complexity. Furthermore, the EM-based iterative estimation converges faster in the second state-space model than in the first one. As a byproduct, the target trajectory can be simultaneously estimated with the measurement bias, after processing a batch of measurements. These results are confirmed by our simulations.

Key words: Non-linear state-space model; Measurement bias; Extended Kalman filter; Extended Kalman smoothing; Expectation-maximization (EM) algorithm

https://doi.org/10.1631/FITEE.1800214　　　　　　　　　　　　　**CLC number:** TP73

1 Introduction

As an emerging type of wireless service, non-stationary target positioning or tracking using the measurements collected in an ad hoc sensor network has drawn considerable attention over the past two decades (Gustafsson and Gunnarsson, 2005; Sayed et al., 2005). Recent research focuses on dealing with the practical environments, i.e., non-line-of-sight (NLOS) environments (Hammes and Zoubir, 2010), multi-path environments (Karunaratne et al., 2012), asynchronous sensors (Li et al., 2006), and uncertain sensor positions (Savic et al., 2016).

In this study, we consider the case where the collected measurements are biased. This can be caused by systematic errors (spatial mis-registration), inaccurate sensor calibration, environmental constraints (NLOS propagation), or other sources. Among these possibilities, it is the additive bias caused by the systematic errors, sometimes called the 'system bias' or 'sensor bias', assumed to be independent of the random measurement error, which is our research interest. In the case of localization of multiple targets (Lin et al., 2004; Okello and Challa, 2004; Lian et al., 2011), the treatment of measurement/sensor bias is known as a problem of sensor registration, which is studied together with multi-track fusion. However,

---

in this study we focus only on the case of a single non-maneuvering target to clearly convey our ideas and present our contributions.

Target tracking using a sensor network is achieved by fusing the complementary information from various sensors. The measurement biases inherent in the sensors will enter into the fusion process and lead to false tracks. Therefore, the effect of those biases must be eliminated by means of estimation and correction.

Estimation of measurement bias has been investigated for decades. In most cases, the bias is assumed to be a constant value. In the standard method, the target state and the measurement biases are separately estimated. For this, the measurement biases are estimated using the least square (LS) (Blackman and Popoli, 1999) and maximum likelihood (ML) (Okello and Ristic, 2003) methods. Alternatively, it is more appropriate to jointly estimate the system biases and target state. Li ZH et al. (2004) proposed that the expectation-maximization (EM) algorithm is incorporated with the Kalman filter to give a simultaneous estimation of the target state and the measurement bias in a state-space linear model. Furthermore, Huang and Leung (2010) proposed that the interacting multiple model (IMM) method is applied to resolve the different behavioral aspects of a maneuvering target. The aforementioned algorithms are off-line algorithms, which usually require batch processing of large amounts of data.

In terms of computational complexity, online algorithms are preferred at the cost of estimation accuracy. Li W et al. (2004) proposed that measurement biases are augmented into the state vector of a state-space model. After that, the biases are estimated with the target state using the unscented Kalman filter. Bugallo et al. (2007) proposed that the marginalized particle filter is used to estimate the target state and measurement biases. The measurement biases are treated as nuisance parameters and are marginalized out. After the target state is estimated using the particle filter, the measurement biases are estimated using the Kalman filter. Zhou et al. (2017) proposed a recursive joint estimation algorithm by carefully coupling the target state and the system biases. The algorithm is qualified to deal with different types of state-space models and measurement biases.

The algorithms discussed in the aforementioned syudies assume that the bias is constant. In this study, we consider a more complicated case; that is, the bias is assumed to be a random variable (the size of bias variance can be determined by the predefined tolerance interval of the Cramer-Rao lower bound), in which case an online algorithm (real-time processing) cannot produce a satisfactory bias estimate. As an alternative, in our treatment, an off-line algorithm (batch processing) is used to estimate the bias. Since the batch processing is based on large measurement (or sample) size in the tracking system, our treatment identifies the unknown system parameter (measurement bias or sensor bias) and estimates the target trajectory with a certain time delay. The time delay is determined by the measurement size used for batch processing. It indicates that our treatment fails to track the target trajectory in real time. Therefore, the bias estimation process involved would be more suitable for an off-line scenario. For example, our treatment can be used to identify the characteristics of measurement bias in the calibration step of a tracking system. After finishing the calibration step and knowing the information about the measurement bias, the tracking system is capable of performing an online target localization.

In this study, the time-of-arrival (ToA) measurement is used and a non-linear state-space model is employed to formulate the tracking problem (Li et al., 2017). To solve the tracking problem, non-linear filtering techniques have to be applied, i.e., an extended Kalman filter (EKF), an unscented Kalman filter, and a particle filter. In this study, we employ the EKF due to its compact formulation. To estimate the measurement bias, statistical estimation algorithms are required, i.e., the LS and ML algorithms. We employ the EM algorithm (Moon, 1996), which is a type of ML algorithm and can be easily integrated with the EKF.

Note that we focus on the special circumstance where the bias is a random variable, which differentiates our work from others. Moreover, rather than proposing novel bias estimation processes or new target tracking algorithms, our primary contribution is analyzing the asymptotic performance of the EM-based bias estimation processes. To the best of our knowledge, we are not aware of any similar work in this area.

Measurement bias is formulated as a random

variable in one state-space model and a determined value in another in our treatment. To estimate the bias, we derive two different EM estimation processes after linearizing the two non-linear state-space models that involve the first-order Taylor expansion. The most important contribution is our study of the asymptotic performance of bias estimation. Assuming a reasonable initial starting point and a sufficiently large measurement size, we theoretically derive the global convergence result of the EM-based measurement bias estimation using the underlying principle of the EM algorithm. Moreover, we study the properties of the two applied state-space models and reveal the link between them.

2 Expectation-maximization-based bias estimation

2.1 Problem formulation

We assume a case where a number of sensors are used to localize a moving radio-active target. The target is moving with the Gauss-Markov random force model in a two-dimensional (2D) plane. It is assumed that ToA measurement can be collected (Gustafsson and Gunnarsson, 2005). Then the tracking problem can be formulated using the following state-space model at time step k (Li and Jilkov, 2003; Gustafsson and Gunnarsson, 2005):

$$\begin{cases} \boldsymbol{x}_k = \boldsymbol{F}\boldsymbol{x}_{k-1} + \boldsymbol{G}\boldsymbol{u}_{k-1}, \\ \bar{\boldsymbol{y}}_k = \boldsymbol{h}(\boldsymbol{x}_k) + \boldsymbol{w}_k, \end{cases} \tag{1}$$

where $\boldsymbol{x}_k = [x_{1,k}, x_{2,k}, \dot{x}_{1,k}, \dot{x}_{2,k}]^{\mathrm{T}}$ is the state vector of the target, containing its instantaneous position $(x_{1,k}, x_{2,k})$ and speed $(\dot{x}_{1,k}, \dot{x}_{2,k})$, and $\bar{\boldsymbol{y}}_k$ is the measurement vector collected from M sensors. In Eq. (1), the transition matrices $\boldsymbol{F}$ and $\boldsymbol{G}$ are defined as

$$\boldsymbol{F} = \begin{bmatrix} \boldsymbol{I}_2 & \Delta t \cdot \boldsymbol{I}_2 \\ \boldsymbol{0}_2 & \boldsymbol{I}_2 \end{bmatrix}, \ \boldsymbol{G} = \begin{bmatrix} \Delta t^2/2 \cdot \boldsymbol{I}_2 \\ \Delta t \cdot \boldsymbol{I}_2 \end{bmatrix}, \tag{2}$$

where $\boldsymbol{I}_2$ denotes an identity matrix of size 2, $\boldsymbol{0}_2$ denotes a null matrix of dimension 2×2, and Δt is the sampling interval. In Eq. (1), $\boldsymbol{h}(\cdot)$ is the non-linear function mapping the state to the measurement. If the ToA measurement is collected, $\boldsymbol{h}(\boldsymbol{x}_k) = [h_1, h_2, \ldots, h_M]^{\mathrm{T}}$ with

$$h_i = \frac{1}{c}\sqrt{(x_{1,k} - s_{1,i})^2 + (x_{2,k} - s_{2,i})^2}, \tag{3}$$

where $i = 1, 2, \ldots, M$. $(s_{1,i}, s_{2,i})$ denotes the position of the ith sensor, and c denotes the propagation velocity of the signal. Assuming that the random force vector $\boldsymbol{u}_k = [u_{1,k}, u_{2,k}]^{\mathrm{T}} \sim \mathcal{N}(\boldsymbol{0}, \boldsymbol{Q})$ and the measurement noise vector $\boldsymbol{w}_k \sim \mathcal{N}(\boldsymbol{0}, \boldsymbol{R})$. $\boldsymbol{u}_k$ and $\boldsymbol{w}_k$ are mutually independent. $\boldsymbol{Q}$ is known a priori (Gustafsson and Gunnarsson, 2005), whereas $\boldsymbol{R}$ is unknown. For simplicity, assuming

$$\boldsymbol{R} = \mathrm{diag}(\beta_1, \beta_2, \ldots, \beta_M), \tag{4}$$

where $\mathrm{diag}(\cdot)$ denotes a square diagonal matrix with the elements in parentheses on the main diagonal. Based on the model in Eq. (1), we can estimate the state $\boldsymbol{x}_k$ using the collected measurement $\bar{\boldsymbol{y}}_k$, i.e., the EKF.

Since the collected measurements are assumed to be biased in our study, the measurement equation in Eq. (1) is re-formulated as

$$\boldsymbol{y}_k = \boldsymbol{h}(\boldsymbol{x}_k) + \boldsymbol{b}_k + \boldsymbol{w}_k, \tag{5}$$

where $\boldsymbol{b}_k$ denotes the measurement bias vector of length M, and $\boldsymbol{y}_k$ denotes the biased measurement compared to the bias-free measurement $\bar{\boldsymbol{y}}_k$ in Eq. (1). The state $\boldsymbol{x}_k$, bias $\boldsymbol{b}_k$, and noise $\boldsymbol{w}_k$ are mutually independent. Therefore, the aim is to identify $\boldsymbol{b}_k$ and estimate $\boldsymbol{x}_k$ simultaneously. In this study, the EM algorithm is employed to identify $\boldsymbol{b}_k$ with the assistance of extended Kalman filtering and smoothing. Considering the practical situations and simplifying the latter theoretical analysis, we make three assumptions as follows:

1. The measurement bias is assumed to be Gaussian distributed, and $\boldsymbol{\Sigma_b}$ in $\mathcal{N}(\boldsymbol{\mu_b}, \boldsymbol{\Sigma_b})$ can be expressed as

$$\boldsymbol{\Sigma_b} = \mathrm{diag}(\alpha_1, \alpha_2, \ldots, \alpha_M). \tag{6}$$

Assume that the biases of different sensors mutually follow independent stationary processes. However, the variances of different sensor biases are quite similar. Both $\boldsymbol{\mu_b}$ and $\boldsymbol{\Sigma_b}$ are unknown.

2. The variance of the measurement bias is smaller than that of the measurement noise, that is, $\alpha_i < \beta_i$, $i = 1, 2, \ldots, M$ (Huang and Leung, 2010; Lian et al., 2011). Meanwhile, the bias variance α_i has a certain amount of uncertainties, and thus the batch processing (smoothing) is needed to accurately estimate it. This is the special case on which we focus.

3. The EM-based estimation process converges to the global maximum in our study; that is, the measurement size is large enough and a reasonable initial starting point is also guaranteed. This is the starting point for our asymptotic analysis of the EM performance in terms of estimating the measurement bias, or simply, the fundamental condition of Lemma 1 is discussed in Section 2.2.

Under these assumptions, we attempt to study the EM-based bias estimation process in terms of two distinct state-space models. Note that a violation of the above assumptions will lead to an unexpected estimation error and make the performance analysis unavailable. The bias is treated as a random variable in model 1 and a constant value in model 2. The details are given in the following subsections.

2.2 Model 1

In this study, the most common way to deal with measurement bias is to augment the bias vector as a part of the state and write the state-space model as

$$\boldsymbol{x}_k = \boldsymbol{F}\boldsymbol{x}_{k-1} + \boldsymbol{G}\boldsymbol{u}_{k-1}, \tag{7}$$
$$\boldsymbol{b}_k = \boldsymbol{b}_{k-1} + \boldsymbol{v}_{k-1}, \tag{8}$$
$$\boldsymbol{y}_k = \boldsymbol{h}(\boldsymbol{x}_k) + \boldsymbol{b}_k + \boldsymbol{w}_k, \tag{9}$$

which is referred to here as model 1. It is known that the bias model in Eq. (8), which is used to track non-stationary bias with time-varying covariance, does not exactly match Assumption 1 in Section 2.1. Nevertheless, the bias model in Eq. (8) can track the stationary bias with Assumption 1. Note that the occurrence of model mismatch can be frequently seen in estimating unknown parameters of the state-space model (Särkkä, 2013). The consequence of the model mismatch in this study will be discussed in Section 3.

The bias evolution noise is defined as $\boldsymbol{v}_k \sim \mathcal{N}(\boldsymbol{0}, \boldsymbol{\Omega})$ with

$$\boldsymbol{\Omega} = \boldsymbol{\Sigma_b} = \mathrm{diag}(\alpha_1, \alpha_2, \ldots, \alpha_M), \tag{10}$$

where $\boldsymbol{\Sigma_b}$ is defined in Eq. (6). In the model in Eqs. (7)–(9), the augmented state vector is $\boldsymbol{z}_k = [\boldsymbol{x}_k^{\mathrm{T}} \ \boldsymbol{b}_k^{\mathrm{T}}]^{\mathrm{T}}$. Defining

$$\tilde{\boldsymbol{F}} = \begin{bmatrix} \boldsymbol{F} & \boldsymbol{0}_{4 \times M} \\ \boldsymbol{0}_{M \times 4} & \boldsymbol{I}_M \end{bmatrix}, \boldsymbol{r}_{k-1} = \begin{bmatrix} \boldsymbol{G}\boldsymbol{u}_{k-1} \\ \boldsymbol{v}_{k-1} \end{bmatrix}, \tag{11}$$

we can rewrite Eqs. (7)–(9) as

$$\boldsymbol{z}_k = \tilde{\boldsymbol{F}}\boldsymbol{z}_{k-1} + \boldsymbol{r}_{k-1}, \tag{12}$$
$$\boldsymbol{y}_k = \tilde{\boldsymbol{h}}(\boldsymbol{z}_k) + \boldsymbol{w}_k, \tag{13}$$

where $\tilde{\boldsymbol{h}}(\boldsymbol{z}_k) = \boldsymbol{h}(\boldsymbol{x}_k) + \boldsymbol{b}_k$.

Note that the covariance matrix $\boldsymbol{R}$ in Eq. (4) of the measurement noise vector $\boldsymbol{w}_k$ is also unknown. Then the work is to simultaneously estimate $\boldsymbol{z}_k$, $\boldsymbol{\Omega}$, and $\boldsymbol{R}$. In Bayesian inference, $\boldsymbol{z}_k$ is treated as a hidden variable, and $\boldsymbol{\Omega}$ and $\boldsymbol{R}$ are treated as unknown parameters of the model. Then the unknown parameter $\boldsymbol{\theta}$ turns out to be the diagonal elements of $\boldsymbol{\Omega}$ and $\boldsymbol{R}$, and it can be expressed as

$$\boldsymbol{\theta} = [\alpha_1, \alpha_2, \ldots, \alpha_M, \beta_1, \beta_2, \ldots, \beta_M]^{\mathrm{T}}. \tag{14}$$

The estimation procedure can be conducted using an EM algorithm. The EM algorithm is a two-step iterative algorithm (Moon, 1996; Tzikas et al., 2008): E-step, in which $Q(\boldsymbol{\theta}, \boldsymbol{\theta}^{\mathrm{old}})$ is computed, and M-step, in which $\boldsymbol{\theta}^{\mathrm{new}} = \arg\max_{\boldsymbol{\theta}} Q(\boldsymbol{\theta}, \boldsymbol{\theta}^{\mathrm{old}})$ is computed. $\boldsymbol{\theta}$ denotes the model parameter to be estimated, e.g., $\boldsymbol{\Omega}$. $Q(\boldsymbol{\theta}, \boldsymbol{\theta}^{\mathrm{old}})$ is defined as

$$Q = \int \log p(\boldsymbol{z}_{1:L}, \boldsymbol{y}_{1:L}; \boldsymbol{\theta}) p(\boldsymbol{z}_{1:L} | \boldsymbol{y}_{1:L}; \boldsymbol{\theta}^{\mathrm{old}}) \mathrm{d}\boldsymbol{z}_{1:L}, \tag{15}$$

where $\log p(\boldsymbol{z}_{1:L}, \boldsymbol{y}_{1:L}; \boldsymbol{\theta})$ is the complete data log-likelihood function, given in Eq. (16) with omission of some irrelevant constant terms, and $p(\boldsymbol{z}_{1:L} | \boldsymbol{y}_{1:L}; \boldsymbol{\theta}^{\mathrm{old}})$ denotes the joint posterior distribution of the states given the parameter $\boldsymbol{\theta}^{\mathrm{old}}$. Assume that the initial state $\boldsymbol{z}_0$ is a determined value. In a rigorous Bayesian method, $\boldsymbol{z}_0$ should be treated as a random vector. In this study, $\boldsymbol{z}_0$ is treated as a determined value so as not to complicate the mathematical formulation and derivation in the sequel. Note that L is the number of observed measurements, which is assumed to be sufficiently large in this study.

$$\begin{aligned}
&\log p(\boldsymbol{z}_{1:L}, \boldsymbol{y}_{1:L}; \boldsymbol{\theta}) \\
&= \sum_{k=1}^{L} \log p(\boldsymbol{z}_k | \boldsymbol{z}_{k-1}, \boldsymbol{\theta}) + \sum_{k=1}^{L} \log p(\boldsymbol{y}_k | \boldsymbol{z}_k, \boldsymbol{\theta}) \\
&= \sum_{k=1}^{L} \log p(\boldsymbol{x}_k | \boldsymbol{x}_{k-1}, \boldsymbol{\theta}) + \sum_{k=1}^{L} \log p(\boldsymbol{b}_k | \boldsymbol{b}_{k-1}, \boldsymbol{\theta}) \\
&\quad + \sum_{k=1}^{L} \log p(\boldsymbol{y}_k | \boldsymbol{z}_k, \boldsymbol{\theta})
\end{aligned}$$

$$= -\frac{L}{2}\log|\boldsymbol{GQG}^{\mathrm{T}}|$$
$$-\frac{1}{2}\sum_{k=1}^{L}(\boldsymbol{x}_k-\boldsymbol{Fx}_{k-1})^{\mathrm{T}}(\boldsymbol{GQG}^{\mathrm{T}})^{-1}(\boldsymbol{x}_k-\boldsymbol{Fx}_{k-1})$$
$$-\frac{L}{2}\log|\boldsymbol{\Omega}|-\frac{1}{2}\sum_{k=1}^{L}(\boldsymbol{b}_k-\boldsymbol{b}_{k-1})^{\mathrm{T}}\boldsymbol{\Omega}^{-1}(\boldsymbol{b}_k-\boldsymbol{b}_{k-1})$$
$$-\frac{L}{2}\log|\boldsymbol{R}|-\frac{1}{2}\sum_{k=1}^{L}\left(\boldsymbol{y}_k-\tilde{\boldsymbol{h}}(\boldsymbol{z}_k)\right)^{\mathrm{T}}\boldsymbol{R}^{-1}\left(\boldsymbol{y}_k-\tilde{\boldsymbol{h}}(\boldsymbol{z}_k)\right).$$
$$(16)$$

By simply inspecting the measurement model in Eq. (9), we can find that simultaneously estimating the variance of the measurement bias $\boldsymbol{b}_k$ and noise $\boldsymbol{w}_k$, i.e., β_i and α_i, seems to be an ill-posed problem; in other words, ambiguity could exist in estimating their variance. In the following, we will elaborate on the EM-based procedure of estimating the unknowns α_i and β_i. After that, we present the trend in evolution of the estimates $\alpha_i^{(n)}$ and $\beta_i^{(n)}$ w.r.t. the increasing EM iteration number n. Interestingly, we will find that the estimates $\alpha_i^{(n)}$ and $\beta_i^{(n)}$ do not approach their respective true values as n increases.

For a linear Gaussian state-space model, the Gaussian distribution $p(\boldsymbol{z}_{1:L}|\boldsymbol{y}_{1:L};\boldsymbol{\theta}^{\mathrm{old}})$ (or its mean and variance) is computed by the Kalman smoother, e.g., the Rauch-Tung-Striebel (RTS) smoother, whereas the log-likelihood function $\log p(\boldsymbol{z}_{1:L},\boldsymbol{y}_{1:L};\boldsymbol{\theta})$ is formulated by logarithm of the product of linear Gaussian components (Eq. (3)) (Shumway and Stoffer, 1982). Subsequently, $Q(\boldsymbol{\theta},\boldsymbol{\theta}^{\mathrm{old}})$ in Eq. (15) is calculated via some matrix calculus steps.

For model 1 in Eqs. (12) and (13), the non-linear measurement model in Eq. (13) should be linearized before calculating $Q(\boldsymbol{\theta},\boldsymbol{\theta}^{\mathrm{old}})$. We do not use a particle filter to cope with the non-linear state-space model due to the following two reasons: (1) The linearization of the non-linear state-space model using the EKF is well established in academia and industry due to its simplicity and satisfactory performance in most tracking problems, although it does introduce some errors. Moreover, the error in our study is not significant as shown in simulation. (2) The EKF results in a compact closed-form solution of $Q(\boldsymbol{\theta},\boldsymbol{\theta}^{\mathrm{old}})$ in Eq. (17), which helps us analyze the estimation performance in Appendix C.

The linearization is twofold: (1) The mean and variance of the distribution $p(\boldsymbol{z}_{1:L}|\boldsymbol{y}_{1:L};\boldsymbol{\theta}^{\mathrm{old}})$

are computed using the extended version of the Kalman filter and smoother, namely, the EKF and extended RTS smoother (see Appendix A); (2) The log-likelihood function $\log p(\boldsymbol{z}_{1:L},\boldsymbol{y}_{1:L};\boldsymbol{\theta})$, or more precisely, the part related to the measurement distribution $\sum_{k=1}^{L}\log p(\boldsymbol{y}_k|\boldsymbol{z}_k,\boldsymbol{\theta})$ in Eq. (16), is approximated by logarithm of the product of linear Gaussian components using the first-order Taylor expansion of $\tilde{\boldsymbol{h}}(\boldsymbol{z}_k)$ (Eq. (B6) in Appendix B).

In Appendix B, we derive the simplified formulation for the function $Q(\boldsymbol{\theta},\boldsymbol{\theta}^{\mathrm{old}})$ by neglecting the terms that do not depend on $\boldsymbol{\theta}$:

$$Q(\boldsymbol{\theta},\boldsymbol{\theta}^{\mathrm{old}}) \approx$$
$$-\frac{L}{2}\log|\boldsymbol{\Omega}|-\frac{1}{2}\mathrm{tr}\left(\boldsymbol{\Omega}^{-1}\left(\boldsymbol{A}-\boldsymbol{B}-\boldsymbol{B}^{\mathrm{T}}+\boldsymbol{C}\right)\right)$$
$$-\frac{1}{2}\mathrm{tr}\left\{\boldsymbol{R}^{-1}\sum_{k=1}^{L}\left[\left(\boldsymbol{y}_k-\tilde{\boldsymbol{h}}(\boldsymbol{z}_k^s)\right)\left(\boldsymbol{y}_k-\tilde{\boldsymbol{h}}(\boldsymbol{z}_k^s)\right)^{\mathrm{T}}\right.\right.$$
$$\left.\left.+\tilde{\boldsymbol{J}}_k\boldsymbol{P}_k^s\tilde{\boldsymbol{J}}_k^{\mathrm{T}}\right]\right\}-\frac{L}{2}\log|\boldsymbol{R}|+\text{constant},$$
$$(17)$$

with

$$\begin{cases}\boldsymbol{A}=\dfrac{1}{L}\sum_{k=1}^{L}\left[\boldsymbol{P}_{k-1}^s+\boldsymbol{b}_{k-1}^s(\boldsymbol{b}_{k-1}^s)^{\mathrm{T}}\right],\\ \boldsymbol{B}=\dfrac{1}{L}\sum_{k=1}^{L}\left[\boldsymbol{P}_{k,k-1}^s+\boldsymbol{b}_k^s(\boldsymbol{b}_{k-1}^s)^{\mathrm{T}}\right], \\ \boldsymbol{C}=\dfrac{1}{L}\sum_{k=1}^{L}\left[\boldsymbol{P}_k^s+\boldsymbol{b}_k^s(\boldsymbol{b}_k^s)^{\mathrm{T}}\right],\end{cases}(18)$$

where $\boldsymbol{P}_k^s$, $\boldsymbol{P}_{k,k-1}^s$, and $\boldsymbol{z}_k^s$ (containing $\boldsymbol{b}_k^s$) are the output of the extended RTS smoother, given in Eq. (A4) in Appendix A as well as $\tilde{\boldsymbol{J}}_k$ given in Eq. (B4) in Appendix B. Note that the terms $\boldsymbol{P}_k^s$, $\boldsymbol{P}_{k,k-1}^s$, and $\boldsymbol{z}_k^s$ are calculated using $\boldsymbol{\theta}^{\mathrm{old}}$. By maximizing $Q(\boldsymbol{\theta},\boldsymbol{\theta}^{\mathrm{old}})$ in Eq. (17) w.r.t. $\boldsymbol{\Omega}$ and $\boldsymbol{R}$, we obtain the estimates at the nth EM iteration:

$$\boldsymbol{\Omega}^{(n)}=\boldsymbol{A}-\boldsymbol{B}-\boldsymbol{B}^{\mathrm{T}}+\boldsymbol{C},(19)$$
$$\boldsymbol{R}^{(n)}=\frac{1}{L}\sum_{k=1}^{L}\left[\left(\boldsymbol{y}_k-\tilde{\boldsymbol{h}}(\boldsymbol{z}_k^s)\right)\left(\boldsymbol{y}_k-\tilde{\boldsymbol{h}}(\boldsymbol{z}_k^s)\right)^{\mathrm{T}}\right.$$
$$\left.+\tilde{\boldsymbol{J}}_k\boldsymbol{P}_k^s\tilde{\boldsymbol{J}}_k^{\mathrm{T}}\right].(20)$$

Since $\boldsymbol{\Omega}^{(n)}$ and $\boldsymbol{R}^{(n)}$ are diagonal matrices as follows:

$$\begin{cases}\boldsymbol{\Omega}^{(n)}=\mathrm{diag}(\alpha_1^{(n)},\alpha_2^{(n)},\ldots,\alpha_M^{(n)}),\\ \boldsymbol{R}^{(n)}=\mathrm{diag}(\beta_1^{(n)},\beta_2^{(n)},\ldots,\beta_M^{(n)}),\end{cases}(21)$$

we obtain

$$\alpha_i^{(n)} = [A]_{ii} - 2[B]_{ii} + [C]_{ii}, \qquad (22)$$

with

$$[A]_{ii} = \frac{1}{L} \sum_{k=1}^{L} \left\{ [\boldsymbol{P}_{k-1}^s]_{(4+i)(4+i)} + ([\boldsymbol{b}_{k-1}^s]_i)^2 \right\},$$

$$[B]_{ii} = \frac{1}{L} \sum_{k=1}^{L} \left\{ [\boldsymbol{P}_{k,k-1}^s]_{(4+i)(4+i)} + [\boldsymbol{b}_k^s]_i [\boldsymbol{b}_{k-1}^s]_i \right\},$$

$$[C]_{ii} = \frac{1}{L} \sum_{k=1}^{L} \left\{ [\boldsymbol{P}_k^s]_{(4+i)(4+i)} + ([\boldsymbol{b}_k^s]_i)^2 \right\}, \qquad (23)$$

and

$$\beta_i^{(n)} = \frac{1}{L} \sum_{k=1}^{L} \left\{ \left[\boldsymbol{y}_k - \tilde{\boldsymbol{h}}(\boldsymbol{z}_k^s) \right]_i^2 + \left[\tilde{\boldsymbol{J}}_k \boldsymbol{P}_k^s \tilde{\boldsymbol{J}}_k^{\mathrm{T}} \right]_{ii} \right\}, \qquad (24)$$

where $[\cdot]_{ii}$ denotes the ith diagonal element of a matrix and $[\cdot]_i$ denotes the ith element of a vector, $i = 1, 2, \ldots, M$.

In summary, we can conduct the EM algorithm of estimating $\boldsymbol{\theta}$ in Eq. (14) in our study via the following iterations:

1. Assume some initial values $\boldsymbol{\theta}^{(0)}$ and set $n = 0$. Do E-step (calculating $\boldsymbol{z}_k^s$, $\boldsymbol{P}_k^s$, and $\boldsymbol{P}_{k+1,k}^s$ using $\boldsymbol{\theta}^{(n)}$ in Eq. (A4)) and M-step (updating the parameter $\boldsymbol{\theta}^{(n+1)}$ in Eqs. (22)–(24)).

2. Set $n = n + 1$ and repeat the E-step and M-step until the estimate $\boldsymbol{\theta}^{(n)}$ is stable.

In Eq. (9), $\boldsymbol{b}_k$ and $\boldsymbol{w}_k$ are assumed to be Gaussian distributed and mutually independent. Then, $\boldsymbol{b}_k + \boldsymbol{w}_k$ could be considered to be an entire noise quantity with Gaussian distribution, whose variance matrix has the diagonal components $\alpha_i + \beta_i, i = 1, 2, \ldots, M$. Therefore, the accurate estimates for the noise variances of $\boldsymbol{b}_k$ and $\boldsymbol{w}_k$ must fulfill the following constraint:

$$\alpha_i^{(n)} + \beta_i^{(n)} \approx \alpha_i + \beta_i, \quad i = 1, 2, \ldots, M, \qquad (25)$$

where α_i and β_i are the true variances of the ith sensor's measurement bias and noise, respectively, which are defined in Eqs. (4) and (10). The equality in Eq. (25) is the most important constraint that the estimation process of $\boldsymbol{\theta}$ has to consider.

Suppose that there is a good initial starting point for $\boldsymbol{\theta}^{(0)}$, namely, $\alpha_i^{(0)}$ and $\beta_i^{(0)}$ in our study, which ensures the EM convergence to the global maximum. In practice, it could be possible to know

the upper bound of the variance of the measurement bias. Thus, we set the initial values $\alpha_i^{(0)}$ and $\beta_i^{(0)}$ higher than their true values. It is obvious that $\alpha_i^{(n)} + \beta_i^{(n)}$ is supposed to approach the true value $\alpha_i + \beta_i$ as the EM iteration repeats, according to the constraint in Eq. (25). Under Assumptions 1–3 in Section 2.1, the behavior of two estimates $\alpha_i^{(n)}$ and $\beta_i^{(n)}$ w.r.t. the EM iteration number is given in Lemma 1:

Lemma 1 After doing enough EM iterations from the initial starting point, generally, the EM estimation decreases $\alpha_i^{(n)}$ and increases $\beta_i^{(n)}$ simultaneously as the iteration number n increases. Finally, the convergence of the EM algorithm is obtained with

$$\begin{cases} \alpha_i^{(n)} \to 0, \\ \beta_i^{(n)} \to \alpha_i + \beta_i, \text{ as } n \to \infty, \end{cases} \qquad (26)$$

which means that the variance of the measurement bias merges into the variance of the measurement noise. The bias estimate is degenerated to a nearly constant value. The proof is given in Appendix C.

Note that it is necessary to re-estimate β_i (i.e., $\boldsymbol{R}$), $i = 1, 2, \ldots, M$, even when it is known. One might argue that it is suboptimal to estimate the known quantity β_i. However, according to the result in Lemma 1, the interaction between the two estimates $\alpha_i^{(n)}$ and $\beta_i^{(n)}$ shows that the estimate $\beta_i^{(n)}$ is definitely not approaching its true value as n increases. If β_i is manually set to its true value during the EM iteration, it is observed from simulations that $\alpha_i^{(n)}$ is reduced to some value smaller than its true $\sigma_{\boldsymbol{b},i}^2$, but not zero, after the EM iteration stops. As a result, the constraint in Eq. (25) is not maintained and the convergence result in Eq. (26) fails to be fulfilled. The EM-based estimation procedure in model 1 gives an inaccurate estimate of the bias and state. Therefore, it is indispensable to estimate β_i and α_i simultaneously in model 1, to capture their mutual influence.

Following the convergence of the EM algorithm in model 1, we can treat the bias vector as a constant vector and further derive the second state-space model.

2.3 Model 2

If the measurement bias vector is treated as a constant vector, the model in Eqs. (7)–(9) is changed

to the following:

$$\begin{cases} \boldsymbol{x}_k = \boldsymbol{F}\boldsymbol{x}_{k-1} + \boldsymbol{G}\boldsymbol{u}_{k-1}, \\ \boldsymbol{y}_k = \boldsymbol{h}(\boldsymbol{x}_k) + \boldsymbol{b} + \boldsymbol{\nu}_k, \end{cases} \quad (27)$$

which is referred to as model 2. The notation can be expressed as

$$\boldsymbol{b} = [b_1, b_2, \ldots, b_M]^{\mathrm{T}}, \quad (28)$$

denoting the constant measurement bias. The integrated measurement noise $\boldsymbol{\nu}_k$ follows the distribution $\mathcal{N}(\boldsymbol{0}, \breve{\boldsymbol{R}})$ with

$$\breve{\boldsymbol{R}} = \mathrm{diag}(\gamma_1, \gamma_2, \ldots, \gamma_M). \quad (29)$$

In model 2, the model parameter $\boldsymbol{\theta}$ contains $\boldsymbol{b}$ and $\breve{\boldsymbol{R}}$, and can be defined as

$$\boldsymbol{\theta} = [b_1, b_2, \ldots, b_M, \gamma_1, \gamma_2, \ldots, \gamma_M]. \quad (30)$$

Similar to model 1, we can derive the function $Q(\boldsymbol{\theta}, \boldsymbol{\theta}^{\mathrm{old}})$ for model 2 by neglecting the terms independent of $\boldsymbol{\theta}$, and it can be expressed as

$$\begin{aligned} &Q(\boldsymbol{\theta}, \boldsymbol{\theta}^{\mathrm{old}}) \\ &= \int \sum_{k=1}^{L} \log p(\boldsymbol{y}_k|\boldsymbol{x}_k, \boldsymbol{\theta}) \cdot p(\boldsymbol{x}_{1:L}|\boldsymbol{y}_{1:L}; \boldsymbol{\theta}^{\mathrm{old}}) \, \mathrm{d}\boldsymbol{x}_{1:L} \\ &\quad + \mathrm{constant} \\ &\approx -\frac{L}{2}\log|\breve{\boldsymbol{R}}| - \frac{1}{2}\mathrm{tr}\Bigg\{ \breve{\boldsymbol{R}}^{-1} \sum_{k=1}^{L} \Bigg[\Big(\boldsymbol{y}_k - \boldsymbol{h}(\boldsymbol{x}_k^s) - \boldsymbol{b}^{(n)}\Big) \\ &\quad \Big(\boldsymbol{y}_k - \boldsymbol{h}(\boldsymbol{x}_k^s) - \boldsymbol{b}^{(n)}\Big)^{\mathrm{T}} + \boldsymbol{J}_k \boldsymbol{P}_k^s \boldsymbol{J}_k^{\mathrm{T}} \Bigg] \Bigg\} + \mathrm{constant}, \end{aligned}$$
$$(31)$$

with $\boldsymbol{J}_k = \partial\boldsymbol{h}(\boldsymbol{x}_k)/\partial\boldsymbol{x}_k|_{\boldsymbol{x}_k=\boldsymbol{x}_k^s}$, differing from $\tilde{\boldsymbol{J}}_k$ in Eq. (B4) in model 1. The joint probability density function (PDF) $p(\boldsymbol{x}_{1:L}|\boldsymbol{y}_{1:L}; \boldsymbol{\theta}^{\mathrm{old}})$ is given in Eq. (D3). $\boldsymbol{x}_k^s$ and $\boldsymbol{P}_k^s$ are the outputs of the extended RTS smoother, given in Eq. (D2) in Appendix D.

By maximizing $Q(\boldsymbol{\theta}, \boldsymbol{\theta}^{\mathrm{old}})$ in Eq. (31) w.r.t. $\boldsymbol{\theta}$ and $\breve{\boldsymbol{R}}$, we obtain the estimate $\boldsymbol{\theta}^{(n)}$ at the nth EM iteration as follows:

$$\begin{cases} \boldsymbol{b}^{(n)} = \Big[b_1^{(n)}, b_2^{(n)}, \cdots, b_M^{(n)}\Big]^{\mathrm{T}}, \\ \breve{\boldsymbol{R}}^{(n)} = \mathrm{diag}\Big(\gamma_1^{(n)}, \gamma_2^{(n)}, \cdots, \gamma_M^{(n)}\Big), \end{cases} \quad (32)$$

with

$$\begin{cases} b_i^{(n)} = \frac{1}{L}\sum_{k=1}^{L}[\boldsymbol{y}_k - \boldsymbol{h}(\boldsymbol{x}_k^s)]_i, \\ \gamma_i^{(n)} = \frac{1}{L}\sum_{k=1}^{L}\Bigg\{ \Big[\boldsymbol{y}_k - \boldsymbol{h}(\boldsymbol{x}_k^s) - \boldsymbol{b}^{(n)}\Big]_i^2 \\ \qquad\qquad + \Big[\boldsymbol{J}_k \boldsymbol{P}_k^s \boldsymbol{J}_k^{\mathrm{T}}\Big]_{ii} \Bigg\}, \end{cases} \quad (33)$$

where $i = 1, 2, \ldots, M$. $[\cdot]_i$ denotes the ith element of a vector, and $[\cdot]_{ii}$ denotes the ith diagonal element of a matrix. It is clear that

$$\begin{cases} b_i^{(n)} \to [\boldsymbol{\mu_b}]_i, \\ \gamma_i^{(n)} \to \alpha_i + \beta_i, \text{ as } n \to \infty, \end{cases} \quad (34)$$

providing that the condition for EM convergence to the global maximum is fulfilled.

If we recall the measurement in Eq. (5), we can find the difference of treating the measurement bias $\boldsymbol{b}_k$ and measurement noise $\boldsymbol{w}_k$ between models 1 and 2. Model 1 considers $\boldsymbol{b}_k$ and $\boldsymbol{w}_k$ as two independent random variables, whereas model 2 regards $\boldsymbol{b}_k$ as a constant and $\boldsymbol{w}_k$ a random variable.

We deduce that the convergence speed is supposed to be smaller in model 1 than in model 2 due to the fact that the number of unknown parameters to be estimated in model 1 is much larger than that in model 2. Specifically, to identify the bias of L measurements, model 1 needs $M \cdot L$ unknowns while model 2 needs only M unknowns. These two models are the same in identifying $\boldsymbol{w}_k$. It is found that the two models approximately have the same convergence results by comparing Eqs. (26) and (34). The bias estimate in model 2 is a constant value while the bias estimates at all time steps in model 1 are nearly equal. That is to say, a great deal of time is needed for the estimates of the random variable $\boldsymbol{b}_k$ in model 1 to be degenerated to a constant value. This result will be proven in Section 3.

Moreover, we can find that the Kalman filter in model 1 has a higher dimension than that in model 2. Since the state in model 1 contains the bias vector of length M in addition to the target position and velocity, the dimension is $M + 4$ in model 1 while 4 in model 2. Model 1 has a higher computational cost than model 2.

3 Simulations

For simulations, we consider an ad hoc sensor network with four stationary sensors. Fig. 1 shows the simulation scenario. The four sensors are located at $[-90, -25]$, $[500, 50]$, $[25, 500]$, and $[450, 500]$ m. Following a Gauss-Markov random force model, the target starts from $[-50, 50]$ m with a driving noise covariance matrix $\boldsymbol{Q} = 0.25\boldsymbol{I}_2$. The initial velocity is $[v_1, v_2]$ where $\sqrt{v_1^2 + v_2^2} = 5$ and v_1 is uniformly selected from the interval

$[0, 5]$. A trajectory example is given in Fig. 1. The sensors record the data sent from the target with a sampling interval of $\Delta t = 0.1$ s. The measurement noise covariance matrix is set as $\boldsymbol{R} = 100\boldsymbol{I}_4$. Note that, in practice, the measurement noise of different sensors depends on the signal-to-noise ratio (SNR) (Hernandez et al., 2006; Stinco et al., 2013) and the diagonal elements of $\boldsymbol{R}$ can differ from each other. Thus, for simplicity, we assume that the sensors have the same SNR. The artificial bias added to the measurements has a mean of $\boldsymbol{\mu_b} = [35, 40, 40, 35]^{\mathrm{T}}$ and a variance of $\Sigma_{\boldsymbol{b}} = 25\boldsymbol{I}_4$. Thus, $\alpha_i = 25$ and $\beta_i = 100$ for $i = 1, 2, \ldots, M$.
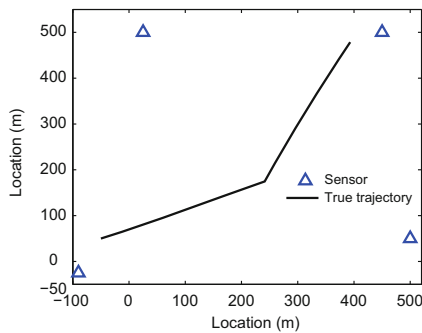

Fig. 1 Sensor locations and target trajectory in the simulation setup

The initial state and covariance matrix for Kalman filtering are given as $\boldsymbol{x}_0 = [x_{1,0}, x_{2,0}, 0, 0]^{\mathrm{T}}$ and $\boldsymbol{P}_0 = \mathrm{diag}(100, 100, 10, 10)$, respectively. For each Monte Carlo simulation, $[x_{1,0}, x_{2,0}]^{\mathrm{T}}$ is randomly drawn from the distribution $\mathcal{N}([-50, 50]^{\mathrm{T}}, 100\boldsymbol{I}_2)$. The initial bias vector and variance matrix for Kalman filtering are given as $\boldsymbol{\mu}_{\boldsymbol{b}0} = [45, 45, 45, 45]^{\mathrm{T}}$ and $\Sigma_{\boldsymbol{b}0} = 100\boldsymbol{I}_4$, respectively, both larger than their true values. The initial values of parameters to be estimated are set as $\boldsymbol{\alpha}^{(0)} = [100, 100, 100, 100]$, $\boldsymbol{\beta}^{(0)} = [200, 200, 200, 200]$, and $\boldsymbol{\gamma}^{(0)} = [300, 300, 300, 300]$. Note that the above initial settings are supposed to ensure the global convergence of the EM estimation. They can be obtained from prior knowledge of the tracking system and some well-known estimation methods (e.g., least squares).

To ease notation, we define the estimate vectors as

$$\begin{cases} \boldsymbol{\alpha}^{(n)} & = [\alpha_1^{(n)}, \alpha_2^{(n)}, \ldots, \alpha_M^{(n)}], \\ \boldsymbol{\beta}^{(n)} & = [\beta_1^{(n)}, \beta_2^{(n)}, \ldots, \beta_M^{(n)}], \\ \boldsymbol{\gamma}^{(n)} & = [\gamma_1^{(n)}, \gamma_2^{(n)}, \ldots, \gamma_M^{(n)}], \end{cases} \quad (35)$$

with their limit values given in Eqs. (26) and (34). In our simulations, the limit value of $\boldsymbol{\alpha}^{(n)}$ is $[0, 0, 0, 0]$. The limit values of $\boldsymbol{\beta}^{(n)}$ and $\boldsymbol{\gamma}^{(n)}$ are both $[125, 125, 125, 125]$, which equals the sum of bias variance (i.e., 25) and measurement noise variance (i.e., 100). In model 1, the EM estimation process gives the estimates $\boldsymbol{\alpha}^{(n)}$, $\boldsymbol{\beta}^{(n)}$, $\boldsymbol{b}_k^s$, and $\boldsymbol{x}_k^s$, whereas in model 2, it gives the estimates $\boldsymbol{\gamma}^{(n)}$, $\boldsymbol{b}^{(n)}$, and $\boldsymbol{x}_k^s$. The EM iteration stops once the Euclidean distance between the variance estimates of the measurements in two consecutive iterations is smaller than a pre-defined threshold 0.01; that is to say, for model 1, $\left| \boldsymbol{\beta}^{(n)} - \boldsymbol{\beta}^{(n-1)} \right| < 0.01$, and for model 2, $\left| \boldsymbol{\gamma}^{(n)} - \boldsymbol{\gamma}^{(n-1)} \right| < 0.01$. The allowed maximum iteration number is set as 1000.

To demonstrate the behavior of the EM estimates $\boldsymbol{\alpha}^{(n)}$, $\boldsymbol{\beta}^{(n)}$, and $\boldsymbol{\gamma}^{(n)}$ w.r.t. the iteration number n, let $\alpha_-^{(n)}$, $\beta_-^{(n)}$, and $\gamma_-^{(n)}$ denote the means of the estimate vector elements:

$$\begin{cases} \alpha_-^{(n)} & = \frac{1}{M} \sum_{i=1}^{M} \alpha_i^{(n)}, \\ \beta_-^{(n)} & = \frac{1}{M} \sum_{i=1}^{M} \beta_i^{(n)}, \\ \gamma_-^{(n)} & = \frac{1}{M} \sum_{i=1}^{M} \gamma_i^{(n)}. \end{cases} \quad (36)$$

Fig. 2 clearly shows the trends of $\alpha_-^{(n)}$ and $\beta_-^{(n)}$ w.r.t. the iteration number n, and Fig. 3 shows the trend of $\boldsymbol{\gamma}_-^{(n)}$ w.r.t. the iteration number n, based on the result of one Monte Carlo running when the sample size is $L = 1000$. In this Monte Carlo running, the EM iteration stops at the 599th iteration in model 1 and the 13th iteration in model 2. Simply speaking, as n increases, $\alpha_-^{(n)}$ gets close to 0, while $\beta_-^{(n)}$ and $\gamma_-^{(n)}$ approach their limit values of 125. This coincides with the convergence results in Eqs. (26) and (34).

Figs. 4–8 show the estimation results of both models w.r.t. the sample size L, based on a simulation of 500 Monte Carlo runnings. We calculated the root mean square error (RMSE) for the estimates. Fig. 4 shows that the estimate in model 2 reaches convergence much faster than that in model 1. Model 1 has a stable estimate after an average of 538 iterations, whereas model 2 has a stable estimate after an average of 14 iterations. Fig 5 shows that the RMSE of estimate vector $\boldsymbol{\alpha}^{(n)}$ (Eq. (35)) is kept at a low level since its limit value is $\boldsymbol{0}$. In Fig. 6, we see that the RMSE of estimate vectors $\boldsymbol{\beta}^{(n)}$ and $\boldsymbol{\gamma}^{(n)}$ (Eq. (35)) decreases as L increases. Fig. 7 shows the RMSE of the bias mean $\boldsymbol{\mu_b}^{(n)}$; that is to say,

$\boldsymbol{\mu}_{\boldsymbol{b}}^{(n)} = \frac{1}{L}\sum_{k=1}^{L} \boldsymbol{b}_k^s$ in model 1, and $\boldsymbol{\mu}_{\boldsymbol{b}}^{(n)} = \boldsymbol{b}^{(n)}$ in model 2. Model 2 estimates $\boldsymbol{\mu}_{\boldsymbol{b}}^{(n)}$ more accurately than model 1. This results in a more accurate estimation of the target positions in model 2 than in model 1 (Fig. 8).
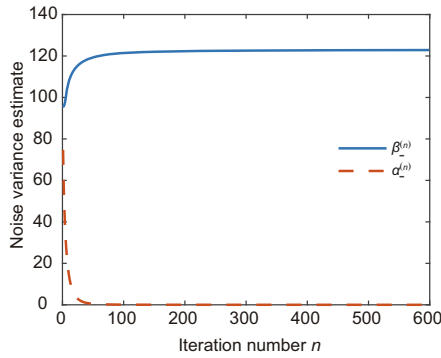

Fig. 2 Estimates $\alpha_-^{(n)}$ and $\beta_-^{(n)}$ of model 1 w.r.t. the iteration number n
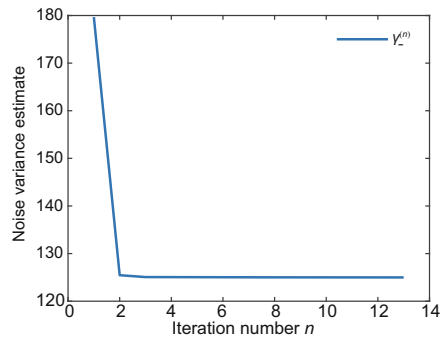

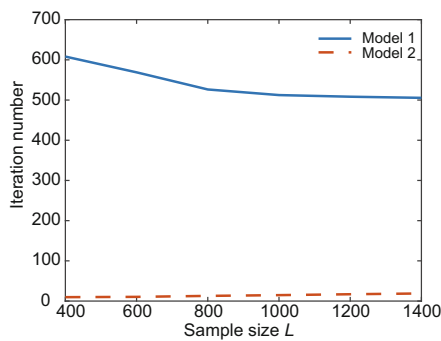**Fig. 3 Estimate $\gamma_-^{(n)}$ of model 2 w.r.t. the iteration number n**

Fig. 4 EM iteration number w.r.t. the sample size L

Although these two models have a similar estimation error for $\boldsymbol{\beta}^{(n)}$ and $\boldsymbol{\gamma}^{(n)}$, model 1 has a larger estimation error for the bias mean $\boldsymbol{\mu}_{\boldsymbol{b}}^{(n)}$ than model 2. This is caused by the fact that the bias model
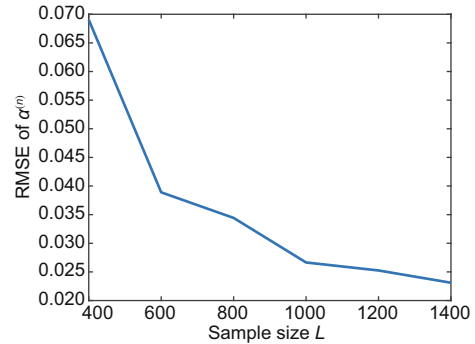
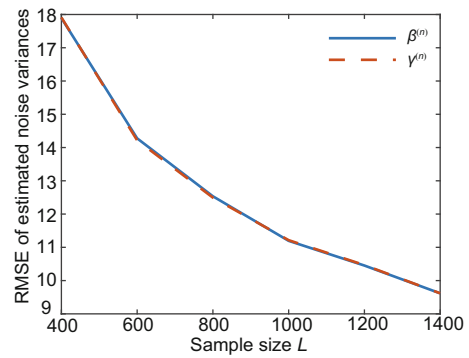**Fig. 5 Root mean square error (RMSE) of $\boldsymbol{\alpha}^{(n)}$ w.r.t. the sample size L**

Fig. 6 Root mean square error (RMSE) of $\boldsymbol{\beta}^{(n)}$ and $\boldsymbol{\gamma}^{(n)}$ w.r.t. the sample size L

in Eq. (8) of model 1, which tracks non-stationary bias with time-varying covariance, does not exactly match the stationary bias with Assumption 1. The estimation error from the model mismatch becomes larger, as the bias variance gets larger. However, the model mismatch would still be acceptable when the bias variance is sufficiently small, which is the reason that the bias model in Eq. (8) is employed in tracking the stationary bias with Assumption 1 (Lian et al., 2011; Särkkä, 2013). Nevertheless, the bias in our case has a larger variance than the one in previous work, which leads to the non-negligible effect of the model mismatch. This is the most important reason for the bias estimation process in model 1 having a relatively poor performance.

It is seen that model 2 reaches convergence faster compared to model 1, while the two models use the same number of measurements in the estimation process. However, model 1 has many more parameters to be estimated than model 2. This is an important reason for model 1 showing an unsatisfactory performance, not only in convergence speed but also in estimation accuracy. When the available measurement size increases, the estimation accuracy
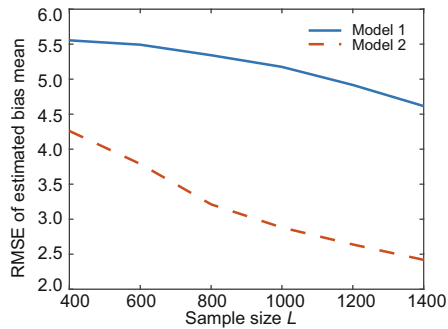
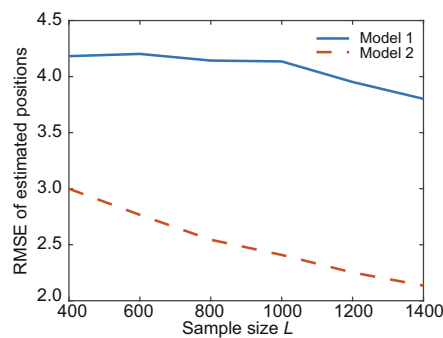Fig. 7 Root mean square error (RMSE) of $\mu_b^{(n)}$ w.r.t. the sample size L

Fig. 8 Root mean square error (RMSE) of estimated target positions w.r.t. the sample size L

of model 1 can be correspondingly improved. The same is valid for model 2. Since model 1 has to estimate more unknown parameters than model 2 does, model 1 will need more measurements than model 2 to achieve the same estimation accuracy.

In Fig. 9, the standard deviations of $\beta^{(n)}$ and $\gamma^{(n)}$ are compared with the square root of the Cramer Rao lower bound (CRLB), which was proposed by Matisko and Havlena (2012). A tighter CRLB for the proposed bias estimators for our study is expected to be derived in the future, by taking the following three points into account: (1) The proposed estimators are essentially the maximum likelihood estimators based on our assumptions; (2) The iterative interaction among the estimates in model 1 exists; (3) The bounds for both bias estimates and noise variance estimates could resort to the hybrid CRLB proposed by Fortunati et al. (2011).

All the simulations require a large number of measurements available for smoothing. Different setups for target tracking demand different measurement sizes. More measurements are necessary in some harsh cases, e.g., complicated target trajectories and initial parameter settings not close to the true ones. If the measurement number or smoothing
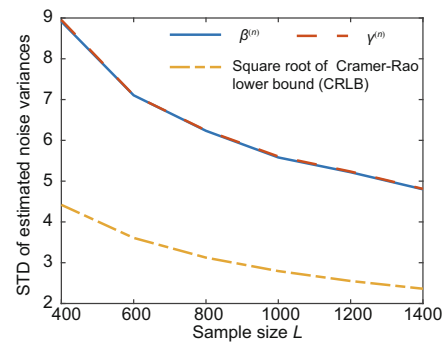

Fig. 9 Standard deviations (STD) of $\beta^{(n)}$ and $\gamma^{(n)}$ w.r.t. the sample size L

window length is small, the above results might not be valid. This is due to the fact that the EM algorithm in our study needs the support of large data size to achieve a good performance and a further global convergence.

Recall that our work aims to study the performance of bias estimation using the EM algorithm in two well-known state-space models under certain circumstances. Our simulations are primarily conducted to validate the derived convergence results for the EM estimation in both models. Our main contribution is a performance analysis of the two proposed EM-based estimation processes. Therefore, a performance comparison of our algorithms and the existing online algorithms for target tracking and parameter estimation is beyond the scope of this study.

4 Conclusions

We have investigated the EM algorithm for estimating the Gaussian measurement bias in two state-space models in the context of target tracking given a bias that is a random variable and a sufficiently large number of measurements. First, we have derived different EM estimation processes for two non-linear state-space models. Both models are linearized via the first-order Taylor expansion, based on extended Kalman filtering and smoothing. The measurement bias and the target state are iteratively estimated. Second, as the most important part of our work, we have analytically derived the global convergence result of the EM-based bias estimation process in model 1 and thoroughly studied the difference between two models. It is shown that model 2 performs better than model 1 in terms of bias estimation. In addition, model 2 has a simpler structure and a faster convergence speed.

References

Blackman S, Popoli R, 1999. Design and Analysis of Modern Tracking Systems. Artech House, Boston, USA.

Bugallo MF, Lu T, Djuric PM, 2007. Bearings-only tracking with biased measurements. Proc 2nd IEEE Int Workshop on Computational Advances in Multi-sensor Adaptive Processing, p.265-268. https://doi.org/10.1109/CAMSAP.2007.4498016

Fortunati S, Farina A, Gini F, et al., 2011. Least squares estimation and Cramér-Rao type lower bounds for relative sensor registration process. *IEEE Trans Signal Process*, 59(3):1075-1087. https://doi.org/10.1109/TSP.2010.2097258

Gustafsson F, Gunnarsson F, 2005. Mobile positioning using wireless networks: possibilities and fundamental limitations based on available wireless network measurements. *IEEE Signal Process Mag*, 22(4):41-53. https://doi.org/10.1109/MSP.2005.1458284

Hammes U, Zoubir AM, 2010. Robust mobile terminal tracking in NLOS environments based on data association. *IEEE Trans Signal Process*, 58(11):5872-5882. https://doi.org/10.1109/TSP.2010.2063425

Haykin S, 2001. Kalman Filtering and Neural Networks. Wiley, New York, USA.

Hernandez ML, Farina A, Ristic B, 2006. PCRLB for tracking in cluttered environments: measurement sequence conditioning approach. *IEEE Trans Aerosp Electron Syst*, 42(2):680-704. https://doi.org/10.1109/TAES.2006.1642582

Huang DL, Leung H, 2010. An EM-IMM method for simultaneous registration and fusion of multiple radars and ESM sensors. In: Mukhopadhyay SC, Leung H (Eds.), Advances in Wireless Sensors and Sensor Networks. Springer Berlin Heidelberg, p.101-124.

Karunaratne BS, Morelande MR, Moran B, 2012. Target tracking in a multipath environment. Proc IET Int Conf on Radar Systems, p.1-6. https://doi.org/10.1049/cp.2012.1645

Li TC, Ekpenyong A, Huang YF, 2006. Source localization and tracking using distributed asynchronous sensors. *IEEE Trans Signal Process*, 54(10):3991-4003. https://doi.org/10.1109/TSP.2006.880213

Li TC, Su JY, Liu W, et al., 2017. Approximate Gaussian conjugacy: parametric recursive filtering under nonlinearity, multimodality, uncertainty, and constraint, and beyond. *Front Inform Technol Electron Eng*, 18(12):1913-1939. https://doi.org/10.1631/FITEE.1700379

Li W, Leung H, Zhou YF, 2004. Space-time registration of radar and ESM using unscented Kalman filter. *IEEE Trans Aerosp Electron Syst*, 40(3):824-836. https://doi.org/10.1109/TAES.2004.1337457

Li XR, Jilkov VP, 2003. Survey of maneuvering target tracking. Part I. Dynamic models. *IEEE Trans Aerosp Electron Syst*, 39(4):1333-1364. https://doi.org/10.1109/TAES.2003.1261132

Li ZH, Chen SY, Leung H, et al., 2004. Joint data association, registration, and fusion using EM-KF. *IEEE Trans Aerosp Electron Syst*, 46(2):496-507. https://doi.org/10.1109/TAES.2010.5461637

Lian F, Han C, Liu W, et al., 2011. Joint spatial registration and multi-target tracking using an extended probability hypothesis density filter. *IET Radar Sonar Navig*, 5(4):441-448. https://doi.org/10.1049/iet-rsn.2010.0057

Lin XD, Bar-Shalom Y, Kirubarajan T, 2004. Exact multi-sensor dynamic bias estimation with local tracks. *IEEE Trans Aerosp Electron Syst*, 40(2):576-590. https://doi.org/10.1109/TAES.2004.1310006

Matisko P, Havlena V, 2012. Cramér-Rao bounds for estimation of linear system noise covariances. *J Mech Eng Autom*, 2(2):6-11. https://doi.org/10.5923/j.jmea.20120202.02

Moon TK, 1996. The expectation-maximization algorithm. *IEEE Signal Process Mag*, 13(6):47-60. https://doi.org/10.1109/79.543975

Okello NN, Challa S, 2004. Joint sensor registration and track-to-track fusion for distributed trackers. *IEEE Trans Aerosp Electron Syst*, 40(3):808-823. https://doi.org/10.1109/TAES.2004.1337456

Okello NN, Ristic B, 2003. Maximum likelihood registration for multiple dissimilar sensors. *IEEE Trans Aerosp Electron Syst*, 39(3):1074-1083. https://doi.org/10.1109/TAES.2003.1238759

Särkkä S, 2013. Bayesian Filtering and Smoothing. Cambridge University Press, Cambridge, UK.

Savic V, Wymeersch H, Larsson E, 2016. Target tracking in confined environments with uncertain sensor positions. *IEEE Trans Veh Technol*, 65(2):870-882. https://doi.org/10.1109/TVT.2015.2404132

Sayed AH, Tarighat A, Khajehnouri N, 2005. Network-based wireless location: challenges faced in developing techniques for accurate wireless location information. *IEEE Signal Process Mag*, 22(4):24-40. https://doi.org/10.1109/MSP.2005.1458275

Shumway RH, Stoffer DS, 1982. An approach to time series smoothing and forecasting using the EM algorithm. *J Time Ser Anal*, 3(4):253-264. https://doi.org/10.1111/j.1467-9892.1982.tb00349.x

Stinco P, Greco MS, Gini F, et al., 2013. Posterior Cramér-Rao lower bounds for passive bistatic radar tracking with uncertain target measurements. *Signal Process*, 93(12):3528-3540. https://doi.org/10.1016/j.sigpro.2013.02.021

Tzikas DG, Likas CL, Galatsanos NP, 2008. The variational approximation for Bayesian inference. *IEEE Signal Process Mag*, 25(6):131-146. https://doi.org/10.1109/MSP.2008.929620

Zhou L, Liu XX, Hu ZT, et al., 2017. Joint estimation of state and system biases in non-linear system. *IET Signal Process*, 11(1):10-16. https://doi.org/10.1049/iet-spr.2015.0068

Appendix A: Extended Kalman filter and extended Rauch-Tung-Striebel (RTS) smoother for model 1

The compact form of the EKF and the fixed-interval extended Rauch-Tung-Striebel (RTS) smoother for model 1 is presented. The detailed derivation can be referred to Haykin (2001) and

Särkkä (2013). If the partial derivative of $\boldsymbol{h}(\boldsymbol{x}_k)$ w.r.t. $\boldsymbol{x}_k$ is given as

$$\boldsymbol{H}_k = \frac{\partial \boldsymbol{h}(\boldsymbol{x}_k)}{\partial \boldsymbol{x}_k}|_{\boldsymbol{x}_k=\boldsymbol{x}_k^-}, \qquad (A1)$$

and we define

$$\begin{cases} \tilde{\boldsymbol{Q}} = \begin{bmatrix} \boldsymbol{GQG}^{\mathrm{T}} & \boldsymbol{0}_{4\times M} \\ \boldsymbol{0}_{M\times 4} & \boldsymbol{\Omega} \end{bmatrix}, \\ \tilde{\boldsymbol{H}}_k = \begin{bmatrix} \boldsymbol{H}_k & \boldsymbol{I}_M \end{bmatrix}, \end{cases} \qquad (A2)$$

then the prediction and update equations of the EKF can be written as

$$\begin{cases} \boldsymbol{z}_k^- = \tilde{\boldsymbol{F}} \boldsymbol{z}_{k-1}^f, \\ \boldsymbol{P}_k^- = \tilde{\boldsymbol{F}} \boldsymbol{P}_{k-1} \tilde{\boldsymbol{F}}^{\mathrm{T}} + \tilde{\boldsymbol{Q}}, \\ \boldsymbol{K}_k = \boldsymbol{P}_k^- \tilde{\boldsymbol{H}}_k^{\mathrm{T}} [\tilde{\boldsymbol{H}}_k \boldsymbol{P}_k^- \tilde{\boldsymbol{H}}_k^{\mathrm{T}} + \boldsymbol{R}]^{-1}, \\ \boldsymbol{z}_k^f = \boldsymbol{z}_k^- + \boldsymbol{K}_k [\boldsymbol{y}_k - \tilde{\boldsymbol{h}}(\boldsymbol{z}_k^-)], \\ \boldsymbol{P}_k = (\boldsymbol{I} - \boldsymbol{K}_k \tilde{\boldsymbol{H}}_k) \boldsymbol{P}_k^-, \end{cases} \qquad (A3)$$

where $\boldsymbol{z}_k^-$ and $\boldsymbol{P}_k^-$ are a priori estimates of the state and its covariance matrix, respectively (Haykin, 2001). Using the Kalman gain $\boldsymbol{K}_k$, a posteriori estimates $\boldsymbol{z}_k^f$ and $\boldsymbol{P}_k$ are updated.

Note that at the $(n+1)^{\mathrm{th}}$ EM iteration, $\boldsymbol{\Omega}$ and $\boldsymbol{R}$ in Eq. (A3) should be replaced by the EM estimates $\boldsymbol{\Omega}^{(n)}$ and $\boldsymbol{R}^{(n)}$ in Eq. (21), respectively.

Furthermore, following the above EKF equations, the backward recursion equations for the fixed-interval extended RTS smoother are obtained as

$$\begin{cases} \boldsymbol{M}_k = \boldsymbol{P}_k \tilde{\boldsymbol{F}}^{\mathrm{T}} \left[\boldsymbol{P}_{k+1}^- \right]^{-1}, \\ \boldsymbol{z}_k^s = \boldsymbol{z}_k^f + \boldsymbol{M}_k \left[\boldsymbol{z}_{k+1}^s - \boldsymbol{z}_{k+1}^- \right], \\ \boldsymbol{P}_k^s = \boldsymbol{P}_k + \boldsymbol{M}_k \left[\boldsymbol{P}_{k+1}^s - \boldsymbol{P}_{k+1}^- \right] \boldsymbol{M}_k^{\mathrm{T}}, \\ \boldsymbol{P}_{k+1,k}^s = \boldsymbol{P}_{k+1}^s \boldsymbol{M}_k^{\mathrm{T}}, \end{cases} \qquad (A4)$$

where $\boldsymbol{M}_k$ is the smoother gain. $\boldsymbol{z}_k^s$ and $\boldsymbol{P}_k^s$ are posteriori smoothed estimates of the state and the covariance, respectively. $\boldsymbol{P}_{k+1,k}^s$ denotes the cross-covariance matrix of $\boldsymbol{z}_{k+1}^s$ and $\boldsymbol{z}_k^s$. Note that Eq. (12.42) in Särkkä (2013) is used to construct the expression for $\boldsymbol{P}_{k+1,k}^s$, instead of Eq. (A11) in Shumway and Stoffer (1982).

It is known that the joint PDF $p(\boldsymbol{z}_{1:L}|\boldsymbol{y}_{1:L};\boldsymbol{\theta}^{\mathrm{old}})$ can be given as

$$p(\boldsymbol{z}_{1:L}|\boldsymbol{y}_{1:L};\boldsymbol{\theta}^{\mathrm{old}}) = \prod_{k=1}^L p(\boldsymbol{z}_k|\boldsymbol{y}_k;\boldsymbol{\theta}^{\mathrm{old}}) \sim \prod_{k=1}^L \mathcal{N}(\boldsymbol{z}_k^s, \boldsymbol{P}_k^s), \qquad (A5)$$

which is the product of Gaussian distributions with the mean $\boldsymbol{z}_k^s$ and covariance $\boldsymbol{P}_k^s$ given in Eq. (A4). Since $\boldsymbol{z}_k = [\boldsymbol{x}_k^{\mathrm{T}} \ \boldsymbol{b}_k^{\mathrm{T}}]^{\mathrm{T}}$, and $\boldsymbol{b}_k$ is independent of $\boldsymbol{x}_k$, the joint PDF $p(\boldsymbol{b}_{1:L}|\boldsymbol{y}_{1:L};\boldsymbol{\theta}^{\mathrm{old}})$ can be readily derived by decomposing the PDF $p(\boldsymbol{z}_{1:L}|\boldsymbol{y}_{1:L};\boldsymbol{\theta}^{\mathrm{old}})$.

Appendix B: Derivation of Eq. (15) for model 1

According to the definition in Eq. (15), $Q(\boldsymbol{\theta}, \boldsymbol{\theta}^{\mathrm{old}})$ is calculated based on $\log p(\boldsymbol{z}_{1:L}, \boldsymbol{y}_{1:L}; \boldsymbol{\theta})$ given in Eq. (16) as well as $p(\boldsymbol{z}_{1:L}|\boldsymbol{y}_{1:L}; \boldsymbol{\theta}^{\mathrm{old}})$ derived in Appendix A. To ease the formulation of $Q(\boldsymbol{\theta}, \boldsymbol{\theta}^{\mathrm{old}})$ in our study, we neglect the terms independent of $\boldsymbol{\theta}$ defined in Eq. (14). Based on Eqs. (15) and (16), we can have

$$\begin{aligned} Q(\boldsymbol{\theta}, \boldsymbol{\theta}^{\mathrm{old}}) = & \int \sum_{k=1}^L \log p(\boldsymbol{b}_k|\boldsymbol{b}_{k-1}, \boldsymbol{\theta}) \cdot p(\boldsymbol{b}_{1:L}|\boldsymbol{y}_{1:L}; \boldsymbol{\theta}^{\mathrm{old}}) \, \mathrm{d}\boldsymbol{b}_{1:L} \\ & + \int \sum_{k=1}^L \log p(\boldsymbol{y}_k|\boldsymbol{z}_k, \boldsymbol{\theta}) \cdot p(\boldsymbol{z}_{1:L}|\boldsymbol{y}_{1:L}; \boldsymbol{\theta}^{\mathrm{old}}) \, \mathrm{d}\boldsymbol{z}_{1:L} \\ & + \text{constant}, \end{aligned} \tag{B1}$$

where $\sum_{k=1}^L \log p(\boldsymbol{b}_k|\boldsymbol{b}_{k-1}, \boldsymbol{\theta})$ and $\sum_{k=1}^L \log p(\boldsymbol{y}_k|\boldsymbol{z}_k, \boldsymbol{\theta})$ are given in Eq. (16).

In model 1, the bias model in Eq. (8) is linear. The first term on the right-hand side of Eq. (B1) can be simply calculated following the second line of Eq. (8) in Shumway and Stoffer (1982), that is,

$$\begin{aligned} & \int \sum_{k=1}^L \log p(\boldsymbol{b}_k|\boldsymbol{b}_{k-1}, \boldsymbol{\theta}) \cdot p(\boldsymbol{b}_{1:L}|\boldsymbol{y}_{1:L}; \boldsymbol{\theta}^{\mathrm{old}}) \, \mathrm{d}\boldsymbol{b}_{1:L} \\ & = -\frac{1}{2} \mathrm{tr}\{ \boldsymbol{\Omega}^{-1} \left[\boldsymbol{A} - \boldsymbol{B} - \boldsymbol{B}^{\mathrm{T}} + \boldsymbol{C} \right] \} - \frac{L}{2} \log|\boldsymbol{\Omega}|, \end{aligned} \tag{B2}$$

where $\boldsymbol{A}$, $\boldsymbol{B}$, and $\boldsymbol{C}$ are given in Eq. (18).

In model 1, the measurement model in Eq. (13) is non-linear. We have to approximate $\log p(\boldsymbol{y}_k|\boldsymbol{z}_k, \boldsymbol{\theta})$ by the logarithm of a linear Gaussian distribution. This can be done via the first-order Taylor expansion of $\tilde{\boldsymbol{h}}(\boldsymbol{z}_k)$. Expanding $\tilde{\boldsymbol{h}}(\boldsymbol{z}_k)$ in a Taylor series at $\boldsymbol{z}_k^s$ and omitting the terms of second order and higher orders, we have

$$\tilde{\boldsymbol{h}}(\boldsymbol{z}_k) \approx \tilde{\boldsymbol{h}}(\boldsymbol{z}_k^s) + \tilde{\boldsymbol{J}}_k(\boldsymbol{z}_k - \boldsymbol{z}_k^s). \qquad (B3)$$

With the Jacobian distribution, we have

$$\begin{cases} \tilde{\boldsymbol{J}}_k = \begin{bmatrix} \boldsymbol{J}_k & \boldsymbol{I}_M \end{bmatrix}, \\ \boldsymbol{J}_k = \frac{\partial \boldsymbol{h}(\boldsymbol{x}_k)}{\partial \boldsymbol{x}_k}|_{\boldsymbol{x}_k=\boldsymbol{x}_k^s}. \end{cases} \quad \text{(B4)}$$

Defining

$$\tilde{\boldsymbol{y}}_k = \boldsymbol{y}_k - \tilde{\boldsymbol{h}}(\boldsymbol{z}_k^s) + \tilde{\boldsymbol{J}}_k \boldsymbol{z}_k^s, \quad \text{(B5)}$$

and substituting Eq. (B3) into the joint logarithmic distribution of the measurements, we obtain

$$\begin{aligned} &\sum_{k=1}^{L} \log p(\boldsymbol{y}_k|\boldsymbol{z}_k,\boldsymbol{\theta}) \\ &= -\frac{L}{2}\log|\boldsymbol{R}| \\ &\quad - \frac{1}{2}\sum_{k=1}^{L} \left(\boldsymbol{y}_k - \tilde{\boldsymbol{h}}(\boldsymbol{z}_k)\right)^{\mathrm{T}} \boldsymbol{R}^{-1} \left(\boldsymbol{y}_k - \tilde{\boldsymbol{h}}(\boldsymbol{z}_k)\right) \\ &\approx -\frac{L}{2}\log|\boldsymbol{R}| \\ &\quad - \frac{1}{2}\sum_{k=1}^{L} \left(\tilde{\boldsymbol{y}}_k - \tilde{\boldsymbol{J}}_k \boldsymbol{z}_k\right)^{\mathrm{T}} \boldsymbol{R}^{-1} \left(\tilde{\boldsymbol{y}}_k - \tilde{\boldsymbol{J}}_k \boldsymbol{z}_k\right), \end{aligned}$$
$$\text{(B6)}$$

which is the logarithm of the product of linear Gaussian components. Using the third and fourth lines of Eq. (8) in Shumway and Stoffer (1982), we obtain the second term on the right-hand side of Eq. (B1), that is,

$$\begin{aligned} &\int \sum_{k=1}^{L} \log p(\boldsymbol{y}_k|\boldsymbol{z}_k,\boldsymbol{\theta}) \cdot p(\boldsymbol{z}_{1:L}|\boldsymbol{y}_{1:L};\boldsymbol{\theta}^{\mathrm{old}}) \,\mathrm{d}\boldsymbol{z}_{1:L} \\ &\approx -\frac{L}{2}\log|\boldsymbol{R}| - \frac{1}{2}\mathrm{tr}\left\{\boldsymbol{R}^{-1} \sum_{k=1}^{L} \left[\left(\tilde{\boldsymbol{y}}_k - \tilde{\boldsymbol{J}}_k \boldsymbol{z}_k^s\right)\right.\right. \\ &\quad \left.\left.\left(\tilde{\boldsymbol{y}}_k - \tilde{\boldsymbol{J}}_k \boldsymbol{z}_k^s\right)^{\mathrm{T}} s + \tilde{\boldsymbol{J}}_k \boldsymbol{P}_k^s \tilde{\boldsymbol{J}}_k^{\mathrm{T}}\right]\right\} \\ &= -\frac{L}{2}\log|\boldsymbol{R}| - \frac{1}{2}\mathrm{tr}\left\{\boldsymbol{R}^{-1} \sum_{k=1}^{L} \left[\left(\boldsymbol{y}_k - \tilde{\boldsymbol{h}}(\boldsymbol{z}_k^s)\right)\right.\right. \\ &\quad \left.\left.\left(\boldsymbol{y}_k - \tilde{\boldsymbol{h}}(\boldsymbol{z}_k^s)\right)^{\mathrm{T}} + \tilde{\boldsymbol{J}}_k \boldsymbol{P}_k^s \tilde{\boldsymbol{J}}_k^{\mathrm{T}}\right]\right\}, \end{aligned}$$
$$\text{(B7)}$$

where the second equation results from inserting $\tilde{\boldsymbol{y}}_k$ (Eq. (B5)). Based on Eqs. (B1), (B2), and (B7), we derive $Q(\boldsymbol{\theta},\boldsymbol{\theta}^{\mathrm{old}})$ in Eq. (17).

Note that the Jacobian $\tilde{\boldsymbol{J}}_k$ in Eq. (B4) differs from $\tilde{\boldsymbol{H}}_k$ in Eq. (A2). The former is calculated at the values $\boldsymbol{x}_k = \boldsymbol{x}_k^s$, whereas the latter is at $\boldsymbol{x}_k = \boldsymbol{x}_k^-$.

Appendix C: Proof of Lemma 1

Before proving Lemma 1, we must point out that the EM estimates $\alpha_i^{(n)}$ and $\beta_i^{(n)}$ do not regularly evolve at the beginning iterations (i.e., small n) as the routine mentioned in this lemma. Instead, they strongly rely on the initial values $\alpha_i^{(0)}$ and $\beta_i^{(0)}$. In our study, the initial values $\alpha_i^{(0)}$ and $\beta_i^{(0)}$ are larger than the true values α_i and β_i, respectively. At the beginning EM iterations, estimates $\alpha_i^{(n)}$ and $\beta_i^{(n)}$ both rapidly decrease to the level of their true values; that is to say, at the n_r^{th} iteration, we have

$$\begin{cases} \alpha_i^{(n_r)} &\approx \alpha_i, \\ \beta_i^{(n_r)} &\approx \beta_i, i = 1, 2, \dots, M. \end{cases} \quad \text{(C1)}$$

We call the EM estimation stage with an iteration number $n < n_r$ the 'starting stage', and the stage where $n > n_r$ the 'regular stage'. Because the EM estimates $\alpha_i^{(n)}$ and $\beta_i^{(n)}$ regularly behave when $n > n_r$, the regular stage is discussed below.

The proof starts from the underlying principle of the EM algorithm. As we know, the mechanism of the EM algorithm can be summarized as follows (Moon, 1996; Tzikas et al., 2008): at the nth EM iteration, an estimate $\boldsymbol{\theta}^{(n)}$ is calculated, and thus $Q(\boldsymbol{\theta}^{(n)},\boldsymbol{\theta}^{(n-1)})$ is not smaller than the counterpart $Q(\boldsymbol{\theta}^{(n-1)},\boldsymbol{\theta}^{(n-2)})$ of the previous iteration; as $Q(\boldsymbol{\theta}^{(n)},\boldsymbol{\theta}^{(n-1)})$ increases with the iteration number n, the likelihood function $p(\boldsymbol{y}_{1:L};\boldsymbol{\theta}^{(n)})$ increases. After sufficient iterations, the EM estimate $\boldsymbol{\theta}^{(n)}$ converges to a maximum likelihood estimate. Thus, we can obtain

$$Q^{(n)} \geq Q^{(n-1)}, \quad \text{(C2)}$$

where $Q^{(n)}$ denotes $Q(\boldsymbol{\theta}^{(n)},\boldsymbol{\theta}^{(n-1)})$ at the nth iteration. The subsequent task is to decompose Eq. (C2) into the terms related to the parameter estimates $\alpha_i^{(n)}$ and $\beta_i^{(n)}$.

By partially substituting Eqs. (19) and (20) into Eq. (17), we obtain

$$\begin{aligned} Q^{(n)} &= -\frac{L}{2}\log|\boldsymbol{\Omega}^{(n)}| - \frac{ML}{2} \\ &\quad - \frac{L}{2}\log|\boldsymbol{R}^{(n)}| - \frac{ML}{2} + \text{constant} \\ &= -\frac{L}{2}\log|\boldsymbol{\Omega}^{(n)}\boldsymbol{R}^{(n)}| + \text{constant}, \end{aligned} \quad \text{(C3)}$$

and furthermore,

$$Q^{(n)} = -\frac{L}{2}\sum_{i=1}^{M} \log \alpha_i^{(n)}\beta_i^{(n)} + \text{constant}, \quad \text{(C4)}$$

where $\alpha_i^{(n)}$ and $\beta_i^{(n)}$ are given in Eqs. (22) and (24), respectively. In Assumption 1 in Section 2.1, the bias variances $\sigma_{\boldsymbol{b},i}^2$ ($i = 1, 2, \ldots, M$) do not significantly differ from each other, which precludes one bias element from having dominating variance and ensures that all M variance estimates evolve at a similar pace. Hence, Eq. (C2) can be expressed as

$$\alpha_i^{(n)}\beta_i^{(n)} \leq \alpha_i^{(n-1)}\beta_i^{(n-1)}, i = 1, 2, \ldots, M. \quad (C5)$$

To check the inequality in Eq. (C5), we denote by $\Delta\alpha_i^{(n)}$ and $\Delta\beta_i^{(n)}$ the incremental or decremental portions of the estimates between two consecutive EM iterations, respectively. Then we can obtain

$$\begin{aligned} \alpha_i^{(n)}\beta_i^{(n)} &= \left(\alpha_i^{(n-1)} + \Delta\alpha_i^{(n-1)}\right)\left(\beta_i^{(n-1)} + \Delta\beta_i^{(n-1)}\right) \\ &= \alpha_i^{(n-1)}\beta_i^{(n-1)} + \alpha_i^{(n-1)}\Delta\beta_i^{(n-1)} \quad (C6) \\ &\quad + \beta_i^{(n-1)}\Delta\alpha_i^{(n-1)} + \Delta\alpha_i^{(n-1)}\Delta\beta_i^{(n-1)}. \end{aligned}$$

It is known that $\Delta\alpha_i^{(n)}$ and $\Delta\beta_i^{(n)}$ are relatively small, that is to say,

$$|\Delta\alpha_i^{(n)}| \ll \alpha_i^{(n)}, |\Delta\beta_i^{(n)}| \ll \beta_i^{(n)}, \quad (C7)$$

especially after a sufficiently large number of iterations. Thus, we could drop the 4th term in Eq. (C6), and have

$$\begin{aligned} \alpha_i^{(n)}\beta_i^{(n)} &\approx \alpha_i^{(n-1)}\beta_i^{(n-1)} \\ &\quad + \alpha_i^{(n-1)}\Delta\beta_i^{(n-1)} + \beta_i^{(n-1)}\Delta\alpha_i^{(n-1)}. \end{aligned}$$
$$(C8)$$

Comparing Eqs. (C5) and (C8), we find that the sum of the last two terms in Eq. (C8) should be non-positive, that is,

$$\alpha_i^{(n-1)}\Delta\beta_i^{(n-1)} + \beta_i^{(n-1)}\Delta\alpha_i^{(n-1)} \leq 0. \quad (C9)$$

Now, we have decomposed the inequality in Eq. (C2) into the one in Eq. (C9), which is related only to the EM estimates $\alpha_i^{(n-1)}$ and $\beta_i^{(n-1)}$, as well as their related terms. Since both $\alpha_i^{(n-1)}$ and $\beta_i^{(n-1)}$ are positive, it is clear that the equality in Eq. (C9) holds for $\Delta\alpha_i^{(n-1)} = \Delta\beta_i^{(n-1)} = 0$ in impling that the EM estimates $\alpha_i^{(n)}$ and $\beta_i^{(n)}$ are stable and that the convergence is achieved. Furthermore, the inequality in Eq. (C9) is valid as long as at least one of $\Delta\alpha_i^{(n-1)}$ and $\Delta\beta_i^{(n-1)}$ is negative.

The regular stage starts from Eq. (C1). Due to $\beta_i > \alpha_i$ (Assumption 2 in Section 2.1), we derive

$$\beta^{(n_r)} > \alpha^{(n_r)}. \quad (C10)$$

To meet the constraint in Eq. (25), for each $n > n_r$, $\alpha_i^{(n)} + \beta_i^{(n)}$ should be close to $\alpha_i + \beta_i$, that is,

$$\begin{aligned} &\alpha_i^{(n-1)} + \beta_i^{(n-1)} \\ &\approx \alpha_i^{(n)} + \beta_i^{(n)} \\ &= \left(\alpha_i^{(n-1)} + \Delta\alpha_i^{(n-1)}\right) + \left(\beta_i^{(n-1)} + \Delta\beta_i^{(n-1)}\right) \\ &\approx \alpha_i + \beta_i, \end{aligned}$$
$$(C11)$$

from which we could obtain

$$\Delta\alpha_i^{(n-1)} \approx -\Delta\beta_i^{(n-1)}. \quad (C12)$$

In other words, the increment or decrement of $\alpha_i^{(n-1)}$ and $\beta_i^{(n-1)}$ compensate for each other. Based on the relationship in Eq. (C12), we obtain two directions in which the EM estimates $\alpha_i^{(n)}$ and $\beta_i^{(n)}$ iteratively evolve:

1. $\Delta\alpha_i^{(n-1)} < 0$ and $\Delta\beta_i^{(n-1)} > 0$, which means that $\alpha_i^{(n)}$ decreases and $\beta_i^{(n)}$ increases as n increases. Due to Eq. (C10), $\beta_i^{(n-1)} > \alpha_i^{(n-1)}$ holds for each n. Considering the relationship in Eq. (C12), we can readily find that the inequality in Eq. (C9) holds. This means that the EM estimation could iteratively go in this direction.

2. $\Delta\alpha_i^{(n-1)} > 0$ and $\Delta\beta_i^{(n-1)} < 0$, which means that $\alpha_i^{(n)}$ increases and $\beta_i^{(n)}$ decreases as n increases. By taking Eqs. (C7), (C10), and (C12) into account, we can find that Eq. (C9) fails at the $(n_r + 1)$th iteration. This means that it is impossible for the EM estimation to iteratively go in this direction.

Based on the statements above, we conclude that the inequality in Eq. (C9) holds when $\Delta\alpha_i^{(n-1)} < 0$ and $\Delta\beta_i^{(n-1)} > 0$, which means that $\alpha_i^{(n)}$ deceases and $\beta_i^{(n)}$ increases compared to their counterparts at the previous iterations. Recall that $\alpha_i^{(n)}$ denotes the variance estimate. Thus, the limit of $\alpha_i^{(n)}$ is zero for a sufficiently large n. Correspondingly, $\beta_i^{(n)}$ approaches $\alpha_i + \beta_i$ as n increases (Eq. (C11)). Therefore, we have the convergence result in Eq. (26).

Appendix D: Extended Kalman filter and extended Rauch-Tung-Striebel (RTS) smoother for model 2

The EKF for model 2 is given as

$$
\begin{cases}
\boldsymbol{x}_k^- = \boldsymbol{F} \boldsymbol{x}_{k-1}^f, \\
\boldsymbol{P}_k^- = \boldsymbol{F} \boldsymbol{P}_{k-1} \boldsymbol{F}^T + \boldsymbol{G} \boldsymbol{Q} \boldsymbol{G}^{\mathrm{T}}, \\
\boldsymbol{K}_k = \boldsymbol{P}_k^- \boldsymbol{H}_k^T [\boldsymbol{H}_k \boldsymbol{P}_k^- \boldsymbol{H}_k^T + \breve{\boldsymbol{R}}]^{-1}, \\
\boldsymbol{x}_k^f = \boldsymbol{x}_k^- + \boldsymbol{K}_k [\boldsymbol{y}_k - \boldsymbol{h}_k(\boldsymbol{x}_k^-) - \boldsymbol{b}], \\
\boldsymbol{P}_k = (\boldsymbol{I} - \boldsymbol{K}_k \boldsymbol{H}_k) \boldsymbol{P}_k^-,
\end{cases}
\tag{D1}
$$

with $\boldsymbol{H}_k$ given in Eq. (A1).

Note that at the $(n+1)^{\mathrm{th}}$ EM iteration, $\boldsymbol{b}$ and $\breve{\boldsymbol{R}}$ in Eq. (D1) should be replaced by the EM estimates $\boldsymbol{b}^{(n)}$ and $\breve{\boldsymbol{R}}^{(n)}$ in Eq. (32), respectively.

The fixed-interval extended RTS smoother for model 2 is given as

$$
\begin{cases}
\boldsymbol{M}_k = \boldsymbol{P}_k \boldsymbol{F}^{\mathrm{T}} \left[\boldsymbol{P}_{k+1}^-\right]^{-1}, \\
\boldsymbol{x}_k^s = \boldsymbol{x}_k^f + \boldsymbol{M}_k \left[\boldsymbol{x}_{k+1}^s - \boldsymbol{x}_{k+1}^-\right], \\
\boldsymbol{P}_k^s = \boldsymbol{P}_k + \boldsymbol{M}_k \left[\boldsymbol{P}_{k+1}^s - \boldsymbol{P}_{k+1}^-\right] \boldsymbol{M}_k^{\mathrm{T}}.
\end{cases}
\tag{D2}
$$

The joint PDF $p(\boldsymbol{x}_{1:L}|\boldsymbol{y}_{1:L}; \boldsymbol{\theta}^{\mathrm{old}})$ can be given as

$$
\begin{aligned}
&p(\boldsymbol{x}_{1:L}|\boldsymbol{y}_{1:L}; \boldsymbol{\theta}^{\mathrm{old}}) \\
&= \prod_{k=1}^{L} p(\boldsymbol{x}_k|\boldsymbol{y}_k; \boldsymbol{\theta}^{\mathrm{old}}) \sim \prod_{k=1}^{L} \mathcal{N}(\boldsymbol{x}_k^s, \boldsymbol{P}_k^s),
\end{aligned}
\tag{D3}
$$

which is the product of Gaussian distributions with mean $\boldsymbol{x}_k^s$ and covariance $\boldsymbol{P}_k^s$ given in Eq. (D2).